Global Biogeochemical Cycles

RESEARCH ARTICLE
10.1029/2020GB006742

Critical Observations of Gaseous Elemental Mercury Air-Sea Exchange

S. Osterwalder[1,2], M. Nerentorp[3], W. Zhu[1], M. Jiskra[4], E. Nilsson[5], M. B. Nilsson[1], A. Rutgersson[5], A. L. Soerensen[6,7], J. Sommar[8], M. B. Wallin[5,9], I. Wängberg[3], and K. Bishop[9]

[1]Department of Forest Ecology and Management, Swedish University of Agricultural Sciences, Umeå, Sweden, [2]Institut des Géosciences de l'Environnement, Université Grenoble Alpes, CNRS, IRD, Grenoble, France, [3]IVL Swedish Environmental Research Institute, Gothenburg, Sweden, [4]Environmental Geosciences, University of Basel, Basel, Switzerland, [5]Department of Earth Sciences, Air, Water and Landscape Science, Uppsala University, Uppsala, Sweden, [6]Department of Environmental Science, Stockholm University, Stockholm, Sweden, [7]Department of Environmental Research and Monitoring, Swedish Museum of Natural History, Stockholm, Sweden, [8]State Key Laboratory of Environmental Geochemistry, Institute of Geochemistry, Chinese Academy of Sciences, Guiyang, China, [9]Department of Aquatic Sciences and Assessment, Swedish University of Agricultural Sciences, Uppsala, Sweden

Abstract Air-sea exchange of gaseous elemental mercury (Hg^0) is not well constrained, even though it is a major component of the global Hg cycle. Lack of Hg^0 flux measurements to validate parameterizations of the Hg^0 transfer velocity contributes to this uncertainty. We measured the Hg^0 flux on the Baltic Sea coast using micrometeorological methods (gradient-based and relaxed eddy accumulation [REA]) and also simulated the flux with a gas exchange model. The coastal waters were typically supersaturated with Hg^0 (mean ± 1σ = 13.5 ± 3.5 ng m^{-3}; ca. 10% of total Hg) compared to the atmosphere (1.3 ± 0.2 ng m^{-3}). The Hg^0 flux calculated using the gas exchange model ranged from 0.1–1.3 ng m^{-2} h^{-1} (10th and 90th percentile) over the course of the campaign (May 10–June 20, 2017) and showed a distinct diel fluctuation. The mean coastal Hg^0 fluxes determined with the two gradient-based approaches and REA were 0.3, 0.5, and 0.6 ng m^{-2} h^{-1}, respectively. In contrast, the mean open sea Hg^0 flux measured with REA was larger (6.3 ng m^{-2} h^{-1}). The open sea Hg^0 flux indicated a stronger wind speed dependence for the Hg^0 transfer velocity compared to commonly used parameterizations. Although based on a limited data set, we suggest that the wind speed dependence of the Hg^0 transfer velocity is more consistent with gases that have less water solubility than CO_2 (e.g., O_2). These pioneering flux measurements using micrometeorological techniques show that more such measurements would improve our understanding of air-sea Hg exchange.

Key Points:

- Mean coastal Hg^0 fluxes measured with micrometeorological methods were similar to fluxes based on Hg^0_{aq} measurements (gas exchange model)
- The gas exchange model predicted Hg^0 emission with a noon peak but flux measurements had no diel peak and periods of Hg^0 uptake
- A cubic relationship between wind speed and the gas transfer velocity was indicated by a subset of the Hg^0 open sea flux measurements

Supporting Information:

Supporting Information may be found in the online version of this article.

Correspondence to:

S. Osterwalder,
stefan.osterwalder@usys.ethz.ch

Citation:

Osterwalder, S., Nerentorp, M., Zhu, W., Jiskra, M., Nilsson, E., Nilsson, M. B., et al. (2021). Critical observations of gaseous elemental mercury air-sea exchange. *Global Biogeochemical Cycles*, *35*, e2020GB006742. https://doi.org/10.1029/2020GB006742

Received 10 JUL 2020
Accepted 11 JUL 2021

1. Introduction

On a global scale 3,800 Mg a^{-1} mercury (Hg) enter the ocean through atmospheric deposition and 300 Mg a^{-1} through riverine input (UNEP, 2019). Atmospheric wet deposition of divalent mercury (Hg^{II}) constitutes the main deposition pathway of total atmospheric Hg to the surface ocean (Zhang et al., 2014), while dry deposition of Hg^{II} constitutes a minor fraction in the mid-latitude marine boundary layer (Holmes et al., 2009). Reduction of Hg^{II} to gaseous elemental mercury (Hg^0) in the surface ocean leads to re-emission of Hg^0 from the ocean of approximately 2,900 Mg a^{-1} (Horowitz et al., 2017). However, these current air-sea Hg exchange estimates are associated with high uncertainty and a better constraint on the Hg^0 flux is crucial for two reasons: first, ocean emissions reduce the reservoir of Hg^{II} available for methylation in the water column and subsequent bioaccumulation in marine biota (Lavoie et al., 2013). Second, ocean emissions increase the amount of Hg actively cycling between the atmosphere, marine and terrestrial ecosystems (Amos et al., 2013; Selin, 2009).

Air-sea exchange of Hg^0 is a diffusion process driven by the concentration gradient between Hg^0 in the atmosphere (Hg^0_{air}) and dissolved gaseous elemental Hg in seawater (DGM, hereinafter referred to as Hg^0_{aq}). The two key factors that control the Hg^0 air-sea exchange are (a) the saturation of Hg^0 in surface water relative to equilibrium conditions expressed by Henry's law constant for Hg^0 and (b) the gas transfer velocity (k) (Qureshi et al., 2011). The Hg^0 flux is typically estimated based on a thin film gas exchange model (Liss & Merlivat, 1986; Wanninkhof, 1992) that uses in situ measurements of Hg^0_{air} and Hg^0_{aq} together with a wind speed dependent parameterization of k that was developed based on field experiments with volatile

and nonvolatile tracers (Nightingale et al., 2000). The water-side gas transfer velocity (k_w) controls the air-sea exchange because Hg^0 has a low water solubility (45 μg L^{-1} at 20°C; Sanemasa, 1975). Photochemical reduction of Hg^{II} in the sea surface water is the dominant driver of Hg^0_{aq} production (Soerensen et al., 2010; Whalin et al., 2007). This makes knowledge of Hg^0_{aq} at the sea-surface an important factor when predicting the seasonal and spatial variability in air-sea exchange. In general, Hg^0_{aq} is determined by purging an inert gas or Hg^0-free air through water from manual discrete samples (Gårdfeldt et al., 2002) or through flowing water using automatic continuous equilibrium systems (CES) (Andersson, Gårdfeldt & Wängberg, 2008). Mean Hg^0_{aq} concentrations in the Atlantic and Pacific Oceans ranged from 6 ng m^{-3} to 26 ng m^{-3} using CES installed on research vessels (Mason et al., 2017; Soerensen et al., 2013, 2014).

Even though Hg^0_{aq} in the sea surface water is extensively characterized, the uncertainties in large scale air-sea Hg exchange estimates remains large due to the lack of direct Hg^0 flux measurements to validate the parameterization of the Hg^0 transfer velocity (Zhang et al., 2019). The Hg^0 transfer velocity is calculated based on the diffusion coefficient of Hg^0 in water (Kuss, 2014) and is parameterized as a function of wind speed (Nightingale et al., 2000). Wind speed is an easily measurable parameter that reflects variability in sea surface turbulence and possibilities for diffusive transport of a gas across the air-sea interface. The relationship between the transfer velocity of CO_2 and wind speed has been suggested to be directly transferable to Hg^0 (Johnson, 2010). This transfer is done by scaling the Schmidt number of Hg^0 to that of CO_2 at the prevailing temperature and salinity conditions (Kuss et al., 2018). However, gases of different solubility respond differently to the processes driving fluxes, so a single wind speed function for all gases is inconsistent with the current understanding of gas transfer physics (Garbe et al., 2014). While wind speed still constitutes the most robust variable to parameterize k, there are other effects that add to the variability in the transfer velocity estimates such as wave breaking, including sea spray and bubble formation, as well as convection (Asher & Wanninkhof, 1998; McNeil & d'Asaro, 2007; Rutgersson et al., 2011; D. Woolf, 1997). Biological film conditions (i.e., surfactants) can also be included in the parameterization (Broecker et al., 1978; Frew, 1997; Soerensen et al., 2013). However, these variables are less easy to measure and wind speed therefore still constitutes the most common predictor variable when calculating air-sea exchange. It has been demonstrated that k for gases with relatively high solubility, such as dimethyl sulfide (DMS), show less wind speed dependence compared to the k of CO_2 (Yang et al., 2011). In contrast, the k of gases with low solubility such as O_2 (about 60 times less soluble than CO_2) indicate a stronger wind speed dependence than for CO_2 (Andersson et al., 2016). In order to constrain air-sea Hg^0 flux estimates an improved parameterization of the relationship between gas transfer velocity for Hg^0 and wind speed is necessary.

Direct field measurements of the Hg^0 flux are needed to evaluate the widely used relationship between the Hg^0 transfer velocity (k_{Hg}) and wind speed. Micrometeorological techniques are commonly used to study air-water exchange of various gases and validate parameterizations that can be used for large scale extrapolations (Garbe et al., 2014). However, for Hg, measurements of Hg^0 fluxes between the atmosphere and water surfaces using micrometeorological methods remains scarce (Sommar et al., 2020).

Here we present the first simultaneous measurement of air-sea Hg^0 exchange using CES, gradient-based and relaxed eddy accumulation (REA) flux methods. These land-based measurements were performed in the Baltic Sea on the islet of Östergarnsholm, using a 30 m tall tower for micrometeorological measurements as well as continuous sampling of Hg^0 in coastal surface water. The objectives of the study were to (a) quantify the Hg^0 air-sea exchange using the gas exchange model and micrometeorological methods in order to assess temporal flux dynamics from coastal waters, (b) compare Hg^0 fluxes from coastal waters and the open sea using REA measurements, and (c) investigate the wind speed dependence of the Hg^0 transfer velocity representative for the open sea.

2. Material and Methods

2.1. Study Site

The study was conducted from May 10 to June 20, 2017 on the islet of Östergarnsholm in the Baltic Sea (57°27′N, 18°59′E), 4 km from the coast of Gotland, Sweden (Figure 1). The Baltic Sea is one of the largest brackish inland seas in the world. The basin was formed by glacial erosion and is thus relatively shallow with an average depth of 54 m (Rosentau et al., 2017). The Baltic Sea covers an area of 392,978 km^2, draining

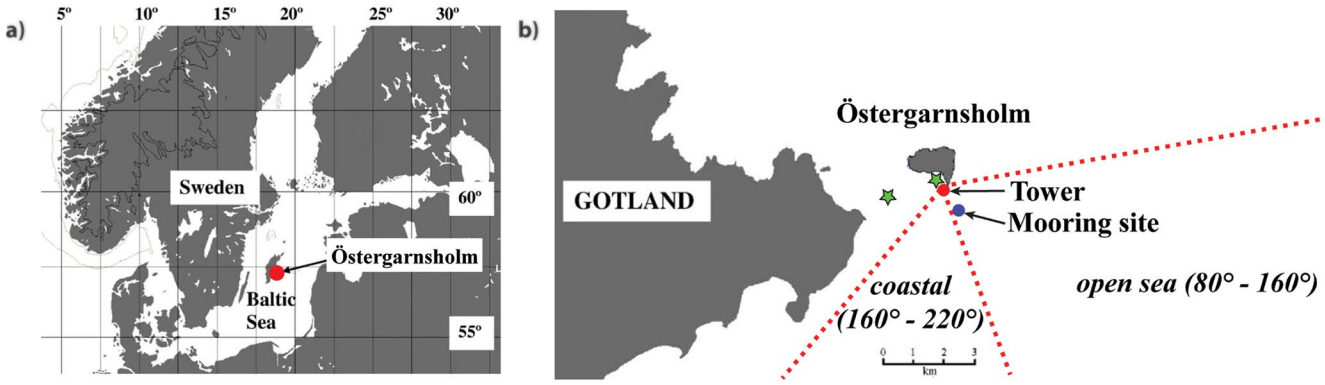

Figure 1. The Östergarnsholm measurement site. The site is indicated on on a (a) large- and (b) small scale map east of the major Baltic island of Gotland. The position of the tower, mooring instrument sensors and the water sampling for total Hg analysis (green stars) are displayed. Directional sectors representing open sea (80°–160°) and coastal (160°–220°) conditions are indicated with red dashed lines. Maps were adapted with permission from Rutgersson et al. (2008).

into the North Sea and the Atlantic Ocean. The salinity ranges from 0.1 g kg^{-1} in the north to 30 g kg^{-1} in the Kattegat (Leppäranta & Myrberg, 2009). The Östergarnsholm research station has been running since 1995, and is part of the Integrated Carbon Observation System Research Infrastructure (ICOS RI) since 2015 (Rutgersson et al., 2020). The station includes a 30 m tall tower with its base 1 ± 0.5 m above mean sea level on the southernmost tip of the flat islet. The tower is equipped with devices for slow response profile measurements of CO_2 and H_2O, wind speed and direction, air temperature, and high frequency instruments for turbulent flux measurements. Other environmental parameters, such as air pressure and solar radiation, were measured at a small hut at the base of the tower. In addition to the land-based measurements, an instrumented mooring located ca. 1 km south-east of the tower (Figure 1) recorded salinity at 5 m depth (SBE 37 SMP-IDO; Seabird Electronics Inc. Bellevue) and sea surface temperature at 0.5 m depth (HOBO; Onset Computer Corp., Boune). Previous land-based micrometeorological flux measurements at the site have found open sea conditions for wind directions (WD) 80° < WD < 160° and coastal conditions for 160° < WD < 220° (Rutgersson et al., 2008, 2020). Manual water samples for total Hg analysis were taken at two sites offshore from the tower ($n = 5$) and between Östergarnsholm and Gotland ($n = 3$) (Figure 1). The seabed in the area is flat and typically at 15–35 m depth. The total Hg analysis was performed by the Swedish Environmental Research Institute (IVL) and followed the US EPA method 1631 (USEPA, 2002).

2.2. Gas Exchange Model: Continuous Equilibrium System

The Hg^0_{aq} concentration in coastal seawater was measured using a continuous equilibrium system (CES) developed by Andersson, Gårdfeldt & Wängberg (2008). For the Hg^0_{aq} measurements, seawater was fed to the CES using a pump fixed ca. 0.5 m under the sea surface, approximately 20 m from the shore. The CES comprises an inner cylinder in which the water is purged with a stream of Hg-free air. The water leaves the inner cylinder in the bottom and flows to an outer cylinder before leaving the system. The purpose of the outer cylinder is to achieve thermal insulation (see Figure S1 in the Supporting Information). The continuous purging air flow rate was 1.6 L min^{-1}. The water flow rate was kept constant at 10.5 L min^{-1}. The equilibrium concentration of Hg^0 established in outgoing air was measured with a time resolution of 5 min using an automatic dual-channel, single-amalgamation cold vapor atomic fluorescence analyzer (Tekran® Model 2537B, Inc.). The air sample flow rate into the instrument was set to 1 L min^{-1} and the excess purging air was ventilated out. A polytetrafluoroethylene (PTFE) filter (0.2 μm pore size, 47 mm diameter) was installed before the Tekran® 2537B intake to prevent particles from entering the instrument and a soda lime trap was installed to remove moisture from the sample air flow. The blanks of the CES were determined by stopping the inflow of water, letting Hg free air purge through the water and deplete Hg^0_{aq}. The detection limit of the subsequently measured Hg^0_{air} by the Tekran® 2537B was 0.5 ng m^{-3}, calculated as three times the standard deviation of the blanks. In a previous application a Hg^0_{aq} sampling efficiency of ca. 99% was reported for the setup (Nerentorp Mastromonaco, 2016). The Tekran® 2537B was calibrated every 25 h using the internal calibration source. The detection limit of the Tekran® 2537 devices is <0.1 ng

m^{-3}. The Hg^0_{aq} concentration and the air-sea Hg^0 flux were calculated following Nerentorp Mastromonaco, Gårdfeldt, and Langer (2017). The flux parameterization includes instantaneous wind speed measured at 10 m height, Henry's Law coefficient for Hg^0 (Andersson, Gårdfeldt, Wängberg & Strömberg, 2008) and a temperature-corrected Schmidt number for CO_2 (Johnson, 2010). The Hg^0 diffusivity was calculated using the Wilke–Chang method (Kuss, 2014). The gas transfer velocity was calculated according to Nightingale et al. (2000) based on air- and seawater-side gas transfer velocities (Fantozzi et al., 2013; Nerentorp Mastromonaco, Gårdfeldt, & Langer, 2017, Nerentorp Mastromonaco, Gårdfeldt, & Wängberg 2017). The full set of equations to calculate the air-sea exchange is given in Table S1 in the Supporting Information.

2.3. Micrometeorological Techniques: Gradient-Based Methods

We measured the Hg^0_{air} concentration alternately at 7 and 29 m for 10 min at each level (2 × 5 min integrated samples) using a Tekran® 2537A. This instrument was placed at the foot of the tall tower and connected to a sampling manifold (Tekran® 1110, synchronized two-port sampler). The manifold was configured to allow the sampling tube, in idle mode, to be continuously flushed by a bypass pump. Both the Tekran® 2537A and the bypass pump operated at a flow rate of 1.3 L min^{-1}. We added a PTFE filter (0.2 μm pore size, 47 mm diameter) at the inlet of both 29 m long sampling tubes made of PTFE. The Tekran® 2537A was automatically calibrated by the internal Hg^0 source every 25 h. The Hg^0 flux (F_{Hg0}) was determined using two different gradient flux methods. The first method was based on both air-side and water-side Hg^0 concentration measurements according to Hintsa et al. (2004). Herein we refer to this method as the water-side gradient method (WGr). The second approach to calculate the Hg^0 flux was only based on air-side Hg^0 concentration measurements as described in Edwards et al. (2005). This method is known as the aerodynamic gradient technique (AGr). For both approaches we calculated the Hg^0 flux according to Equation 1:

$$F_{Hg0} = -\frac{k \cdot u_* \cdot z}{\phi_h\left(\frac{z}{L}\right)} \cdot \frac{\delta C}{\delta z} \tag{1}$$

where k is the Karmen constant (0.4), u* the friction velocity, z the measurement height, $\phi_h\left(\frac{z}{L}\right)$ the universal temperature profile, L the Monin-Obukhov length and δC the Hg^0 concentration difference between two heights ($z_1 = 7$ m and $z_2 = 29$ m). In the first approach we determined the Hg^0 flux (F_{WGr}) by fitting a hyperbolic tangent function to Hg^0_{aq} and Hg^0_{air} concentrations measured at the two heights following Gualtieri and Mihailović (2008):

$$C = \left(C_{bulk} - C_{surface}\right) \cdot A \cdot \tanh\left(\frac{B}{A} \cdot z\right) + C_{surface} \tag{2}$$

where C_{bulk} is the asymptotic atmospheric concentration value of Hg^0_{air} approached far from the surface, which will be close to the measured value at 29 m because the largest gradient is close to the sea surface. $C_{surface}$ is the Hg^0_{aq} concentration. The fitting coefficient A was set to unity which results in $C = C_{surface}$ at the surface and $C = C_{bulk}$ as the measurement height (z) becomes large. B is the free parameter that was solved for using a nonlinear least squares method based on the three concentration measurements (Hg^0_{air} in 7 and 29 m height and Hg^0_{aq}). To calculate F_{WGr} the Hg^0_{air} concentration (C) and local gradient was obtained from the curve fit at 10 m height. At this height a sonic anemometer was installed that allowed the co-located estimates of turbulence parameters. If only air-side measurements are available the second approach (aerodynamic gradient method) can still provide flux estimates by estimating the gradient by a finite difference approximation. Hence, we derived the aerodynamic gradient flux (F_{AGr}) using the two Hg^0_{air} concentration measurements only (Equation 1). For both approaches data were rejected during non-stationary conditions (36% of the data). These periods were identified when key parameters changed more than about 1.5 m s^{-1} (wind speed), 0.74 K (virtual potential temperature), 30 W m^{-2} (buoyancy flux), 0.13 m s^{-2} (friction velocity), 0.07 ng m^{-3} (scalar concentrations) and 16 ng m^{-2} s^{-1} (fluxes) from F_{AGr} during any 40 min period. These limits were chosen based on 90th percentile values of time differences to flag the most non-stationary data similar to the approaches of Foken and Wichura (1996) and Honkanen et al. (2018). The calculation of F_{WGr} was mostly determined by the difference between Hg^0_{aq} and Hg^0_{air} measured at 7 m height. Thus the concentration difference was large enough to be resolved during the entire campaign. The minimum resolvable

Hg^0 concentration gradient to calculate F_{AGr} was derived from intermittent Hg^0_{air} measurements ($n = 137$) with the sampling line inlets mounted side by side at 7 m height on the tower. The mean of the Hg^0_{air} concentration difference plus one standard deviation, was 0.02 ng m^{-3}. Subsequently 43% of the gradients were resolvable. This threshold was similar to that of previous studies on terrestrial Hg^0 fluxes measured using gradient-based methods: 0.01 ng m^{-3} (Edwards et al., 2005), 0.02 ng m^{-3} (Fritsche et al., 2008), 0.02 ng m^{-3} (MacSween et al., 2020), 0.06 ng m^{-3} (Zhu et al., 2015) and 0.07 ng m^{-3} (Converse et al., 2010). As done in these earlier studies, Hg^0 flux data falling below this threshold were not removed from data analysis because this would overestimate mean exchange rates (Fritsche et al., 2008; MacSween et al., 2020). Herein we use the term Hg^0 uptake to the sea surface rather than Hg^0 dry deposition because uptake indicates a physical process in which atmospheric Hg^0 is dissolved in water and eventually oxidized to Hg^{II}.

2.4. Micrometeorological Techniques: Relaxed Eddy Accumulation

The dual-inlet, single detector relaxed eddy accumulation (REA) system was connected to a sonic anemometer CSAT3 (Campbell Scientific) mounted at the tip of a 3.5 m bar attached to the tower, 10 m above the base pointing southwards. The REA system consists of a set of fast-response valves to sample and separate vertically upward and downward moving air parcels, Hg^0_{air} adsorption cartridges, an atomic fluorescence analytical unit as well as a Hg^0 reference gas and Hg zero-air generator unit (Osterwalder et al., 2016; 2017; 2018). The Hg^0 flux was calculated over 30 min intervals using:

$$F_{Hg0} = \beta\sigma_w\left(\overline{C_u} - \overline{C_d}\right) \tag{3}$$

where σ_w is the standard deviation of the vertical wind velocity, $\overline{C_u} - \overline{C_d}$ is the difference between the mean Hg^0_{air} concentration in updrafts and downdrafts, respectively. β is the relaxation coefficient determined by the Eddy covariance sensible heat flux ($\overline{w'T'}$) according to:

$$\beta = \frac{\overline{w'T'}}{\sigma_w\left(\overline{T_u} - \overline{T_d}\right)} \tag{4}$$

where $\overline{T_u} - \overline{T_d}$ is the difference between updraft and downdraft air temperatures. We applied a recursive high pass filter to remove bias in measurements of the vertical wind velocity (Osterwalder et al., 2016) and a dynamic deadband ($0.5\,\sigma_w$), which enabled the use of a constant β-value of 0.51 (Grönholm et al., 2008). The system was continuously calibrated (each cartridge once per hour) with different volumes of automatically injected Hg^0 saturated air. Recovery of Hg^0 was determined after the campaign by manual syringe injections of different volumes of Hg^0 vapor from an external Hg source (Tekran® Model 2,505). Data were analyzed and treated according to Osterwalder et al. (2016) and rejected during very stable conditions ($z/L > 2$) (3%). The sampling line bias was tested by applying a 2 s simulated wind signal system. From there a minimum detectable Hg^0 concentration difference was derived based on the absolute standard deviation of the residuals from orthogonal linear regression fitting (Zhu et al., 2015). There was no trend in the relationship between the residuals and time or Hg^0_{air} concentration ($n = 88$). The minimum detectable Hg^0 concentration difference (1σ) was 0.06 and 0.07 ng m^{-3} for cartridge pairs 1 and 2, respectively. For all the fluxes calculated from cartridge pair 1% and 2%, 64% and 57% of the measured Hg^0 flux differences were above these limits, respectively. For the costal and open sea sector, fluxes were above the threshold in 59% and 54% of the cases, respectively. Please note that the reported fluxes include all data since magnitudes of average exchange rates would otherwise be overestimated.

2.5. Calculation of the Hg^0 Air-Sea Transfer Velocity

The Hg^0 transfer velocity (k_{Hg}) was calculated by solving the flux equation in the gas exchange model for k_{Hg} (cp. Table S1):

$$k_{Hg} = \frac{F_{Hg^0}}{\left(Hg^0_{aq} - \frac{Hg^0_{air}}{H'}\right)} \tag{5}$$

where F_{Hg0} is the measured Hg^0 flux with REA, Hg^0_{aq} the Hg^0 concentration in the sea surface water and Hg^0_{air} the Hg^0 concentration in the air. H′ denotes the Henry's law coefficient for Hg^0. Calculations of k_{Hg} under different sea surface temperature and salinity conditions were made comparable by normalization with respect to the Schmidt number (Sc):

$$k_{660} = k_{Hg}\left(\frac{Sc_{Hg}}{660}\right)^{-0.5} \quad (6)$$

The Schmidt number describes the ratio of the kinematic viscosity of water and the diffusion rate of a gas of interest (in our case Hg^0) across the air-sea boundary (Johnson, 2010). The transfer velocity k_{660} is scaled to the Schmidt number for CO_2 of 660 determined in seawater at 20°C.

2.6. Wind Speed Dependence of the Air-Sea Transfer Velocity

The wind speed dependence of k_{660}-normalized transfer velocities for Hg^0 was compared to parameterizations presented in Nightingale et al. (2000), Liss and Merlivat (1986), Wanninkhof and McGillis (1999), McGillis et al. (2001), Wanninkhof (2014) and Andersson et al. (2016). Furthermore the air-sea transfer velocity was determined using the physically based Coupled Ocean-Atmosphere Response Experiment flux algorithm with CO_2 (COAREG3.6) (Fairall et al., 2011). The wind dependence of the transfer velocity was determined over the course of the entire sampling campaign using the MATLAB algorithm that is available here: https://www.pmel.noaa.gov/ocs/flux-documentation.

2.7. Data Analysis

Statistical analysis was performed using *R* version 4.0.0 (R Foundation for Statistical Computing). Descriptive statistics of Hg^0 concentrations and flux measurements are expressed as mean ± standard deviation (1σ). Additionally, the range from the 10th to the 90th percentiles are given. The non-parametric unpaired two-samples Mann-Whitney U test was used to compare significant differences between two groups of data (e.g., concentrations, fluxes). The relative importance of the various environmental parameters driving Hg^0_{aq} or Hg^0 fluxes was examined using stepwise generalized linear models. Spearman correlation coefficient (ρ) between half-hourly values of Hg^0 concentrations, Hg^0 fluxes and environmental variables are given. Unless stated otherwise, the significance level was 5% (p-value < 0.05).

3. Results

3.1. Environmental Conditions

From the start (May 10, 2017) to the end (June 20, 2017) of the measurement campaign the length of daylight increased from 15.5 to 17.0 h. Daytime mean solar radiation (Rg) was 381 Wm^{-2} (max. hourly mean = 702 Wm^{-2} [12:00]). The daily mean ± 1σ air temperature increased from 2.4 ± 0.5°C (10 May) to 18.2 ± 3.5°C (18 June). Environmental parameters used in the Hg^0 air-sea exchange model include sea surface temperature (SST), sea surface salinity (SSS), wind speed (u_{10}), atmospheric pressure (Pres), dissolved gaseous mercury (Hg^0_{aq}) (Figure 2) and gaseous elemental mercury (Hg^0_{air}) (Figure 3). The daily mean SST ranged from 6.5 ± 0.1°C (10 May) to 15.6 ± 0.3°C (19 June) and the SSS ranged between 7.05 g kg^{-1} and 7.29 g kg^{-1} (Figure 2a). The mean daytime (Rg ≥ 5 W m^{-2}) and nighttime (Rg < 5 W m^{-2}) u_{10} was 5.4 ± 2.5 m s^{-1} (range 0.2–14.7 m s^{-1}) and 4.7 ± 2.2 m s^{-1} (range 0.3–11.6 m s^{-1}), respectively. The Pres ranged from 992 hPa to 1,029 hPa (Figure 2b). During the study period the wind direction was from the open sea (80° < WD < 160°) 21% of the time and from the coastal sector (160° < WD < 220°) 31% of the time.

3.2. Atmospheric Hg^0 Concentrations

Concentrations of Hg^0_{air} at 7 and 29 m were 1.27 ± 0.2 ng m^{-3} and 1.30 ± 0.4 ng m^{-3} (mean ± 1σ), respectively. We found no difference between the two heights when considering the whole day or when separately comparing day (median = 1.23 and 1.25 ng m^{-3}) or night (median = 1.24 and 1.24 ng m^{-3}; $p > 0.05$) measurements (Figure 3). The Hg^0_{air} concentrations were relatively constant throughout the day with the

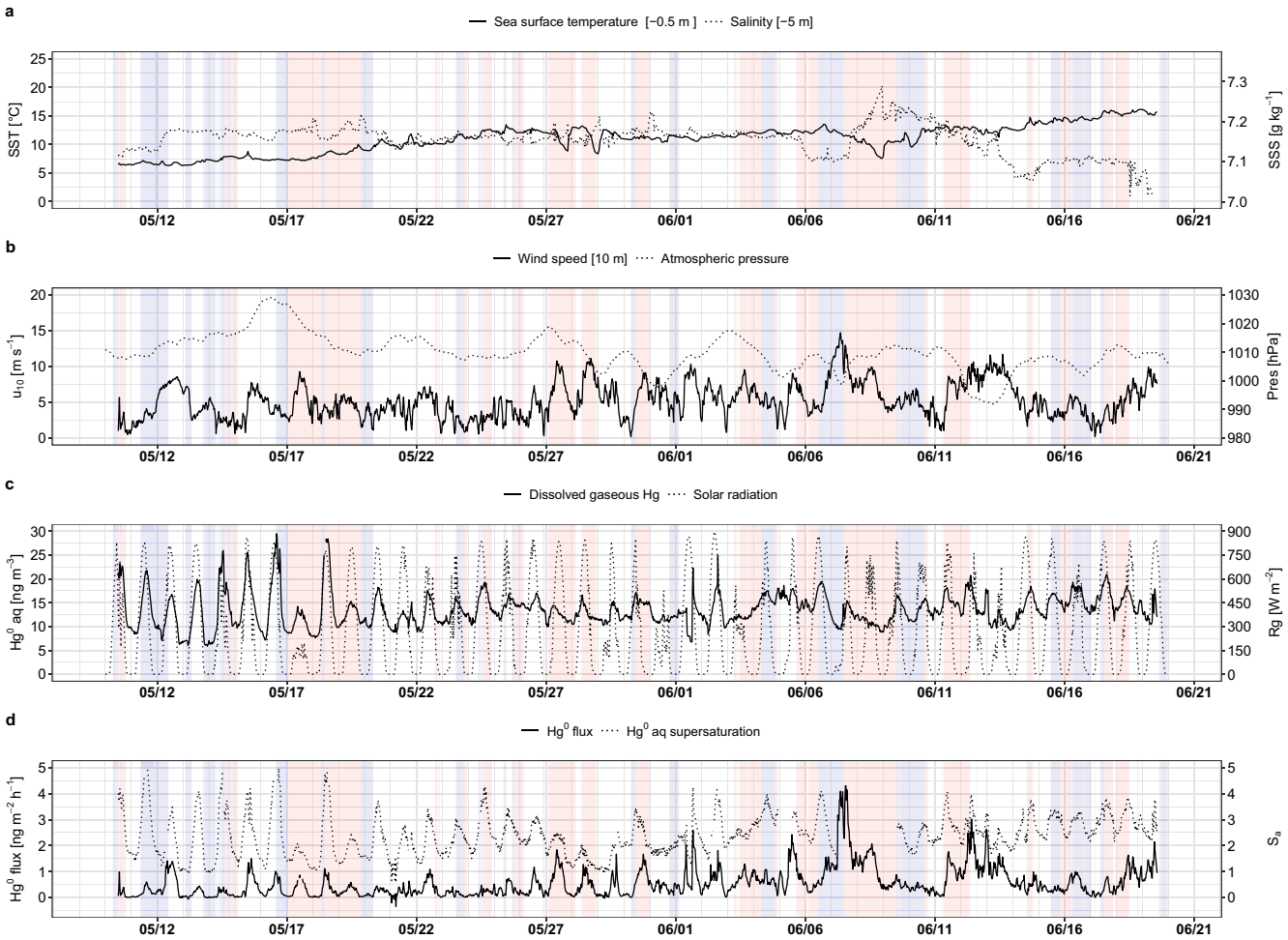

Figure 2. Time series of environmental parameters used in the Hg^0 air-sea exchange model and solar radiation. (a) sea surface temperature at 0.5 m and salinity at 5 m below sea surface, (b) wind speed at 10 m height and atmospheric pressure, (c) dissolved Hg^0_{aq} and solar radiation (d) Hg^0 flux calculated with the gas exchange model and the degree of saturation of dissolved Hg^0. The shaded area indicates wind directions from the open sea sector (80°–160°, blue) and coastal sector (160°–220°, red).

10th and 90th percentiles being 1.06 and 1.45 ng m^{-3} at 7 m and being 1.09 and 1.46 ng m^{-3} at 29 m (Figure 4a). Our measurements compare well with a mean Hg^0_{air} concentration of 1.29 ± 0.14 ng m^{-3} (range from 0.8 ng m^{-3} to 1.84 ng m^{-3}) measured on a ship passing west of Gotland while traveling from the north (Luleå) to south (Landskrona) of the Baltic Sea between April 28 and May 5, 2017 (Hoglind et al., 2018) and 1.2 ± 0.4 ng m^{-3} determined during cruises passing the Eastern Gotland Sea between 2011 and 2015 (Kuss et al., 2018).

3.3. Total Hg and Dissolved Hg^0 Concentrations

Mean total seawater Hg concentrations (Hg_{tot}) of 0.13 ± 0.01 ng L^{-1} (0.6 ± 0.05 pM) were measured in discrete samples at about 0.5 m depth (n = 8). The concentrations were at the lower end of the range (0.1–2.1 ng L^{-1}, mean = 0.4 ± 0.4 ng L^{-1}) reported for the Baltic Sea (Soerensen et al., 2018). Mean concentrations of Hg^0_{aq} in the sea surface water at ca. 0.5 m depth were 13.5 ± 3.5 ng m^{-3} ranging between 9.7 and 17.7 ng m^{-3} (10th and 90th percentile) (Figure 2c). Surface water Hg^0_{aq} concentrations were more variable than Hg^0_{air}. The observed range of Hg^0_{aq} was in good agreement with concentrations ranging from 10 to 25 ng m^{-3} reported for the eastern and western Gotland Sea and the Bornholm Sea in May 2013 (Kuss et al., 2018). A larger mean Hg^0_{aq} concentration of 54 ± 28 ng m^{-3} was measured in July 2016 during a cruise in the southern Baltic Sea (Soerensen et al., 2018). In our study, mean Hg^0_{aq} concentrations during the

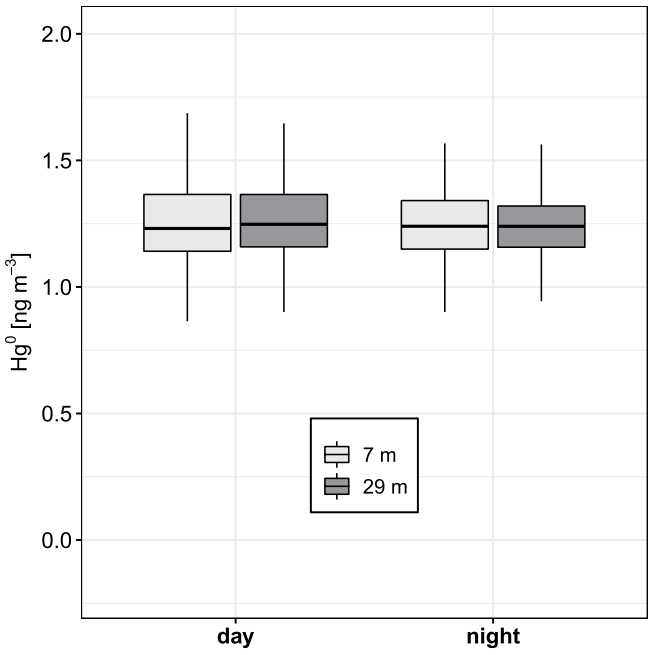

Figure 3. Comparison of daytime and nighttime Hg^0_{air} concentrations at 7 and 29 m height above the sea surface. The bold line in the box represents median values. The horizontal border lines indicate the 25th (Q1) and 75th (Q3) percentiles, from bottom to top. The lower whisker marks Q1 minus 1.5 times the interquartile range (IQR). The upper whisker marks Q3 plus 1.5 IQR. Outliers are not displayed.

day (14.3 ng m^{-3}) were elevated by 23% compared to nighttime (11.6 ng m^{-3}; $p < 0.05$). To examine the drivers of the diel pattern we analyzed possible environmental factors by comparing 30 min variability of Hg^0_{aq} concentration and selected model parameters after stepwise regression. The best model, including solar radiation, sea surface temperature and wind speed, explained only 37% of the variance in Hg^0_{aq} concentration ($r^2 = 0.37$, $p < 0.05$). This indicates that we miss important environmental drivers of Hg^0_{aq} concentration and production or that the response to these drivers was delayed.

3.4. Hg^0 Flux Derived From the Gas Exchange Model

The Hg^0_{aq} concentration was supersaturated relative to Hg^0_{air} during 99% of the study period. The median Hg^0_{aq} supersaturation was 233% (Figure 2d). Highest and lowest hourly median Hg^0_{aq} supersaturation was 321% and 169%, recorded at 11:30 and 04:30, respectively. Also during the night, supersaturation of Hg^0_{aq} was predominant (98%), causing a net Hg^0 flux into the atmosphere. The mean Hg^0 flux was 0.6 ± 0.6 ng m^{-2} h^{-1} ($n = 1918$) and ranged between 0.1 ng m^{-2} h^{-1} and 1.3 ng m^{-2} h^{-1}. The Hg^0 flux showed a distinct diel cycle with higher median daytime (0.64 ng m^{-2} h^{-1}) than nighttime fluxes (0.35 ng m^{-2} h^{-1}; $p < 0.05$) (Figure 4d). Hg^0_{aq} concentrations and wind speed (representing the link to the transfer velocity) were also higher during the day ($p < 0.05$, Figures 4a and 4c).

3.5. Hg^0 Flux From Gradient-Based Measurements

We calculated the Hg^0 flux using two different gradient methods, the water-air gradient-based method (WGr) and the aerodynamic gradient method (AGr). Using WGr we calculated a mean Hg^0 flux of 0.5 ± 1.1 ng m^{-2} h^{-1} and using AGr the flux was 0.3 ± 3.9 ng m^{-2} h^{-1} (Figure 5). The WGr that uses the surface (water-side) Hg^0 concentration in addition to the atmospheric concentration shows emissions from the sea-surface consistent with the larger observed concentration difference between air and water. The F_{WGr} indicated that Hg^0 emissions were occurring 37% of the time (>0.1 ng m^{-2} h^{-1}) while the flux was close to zero (<0.1 ng m^{-2} h^{-1}) the rest of the time. The F_{AGr} showed a varying sign of positive (upward) and negative (downward) fluxes. The flux indicated sea surface Hg^0 uptake 53% of the time. The Hg^0 fluxes were in general stronger during periods of water to air transfer than the opposite direction, resulting in the overall net transfer from water to air.

3.6. Hg^0 Flux From REA Measurements

The average half-hourly Hg^0 flux measured with the REA system (F_{REA}) was 0.6 ± 37 ng m^{-2} h^{-1} for the coastal sector and 6.3 ± 36 ng m^{-2} h^{-1} for the open sea sector (Figure 5). Downward Hg^0 fluxes were observed 45% (coast) and 35% (open sea) of the time, indicating Hg^0 uptake. Despite the larger flux variability observed when using micrometeorological flux techniques, the mean Hg^0 flux over the coastal Baltic Sea during the study period was not different between F_{WGr}, F_{AGr}, and F_{REA} ($p > 0.05$). In contrast to the fluxes calculated with the gas exchange model, none of the Hg^0 fluxes measured with micrometeorological methods (F_{WGr}, F_{AGr}, F_{REA}; see time series in Figure S2 in the Supporting Information) showed a statistically significant diel pattern ($p > 0.05$; Figures 4e–4g).

3.7. Wind Speed Dependence of k_{Hg}

In order to investigate the wind speed dependence of k_{Hg}, we therefore extracted a subset of F_{REA} with a large range of wind speeds from a period with relatively constant wind direction from the open sea sector. We did this because 90% of the wind speed data were below 6.9 m s^{-1} for open sea conditions and

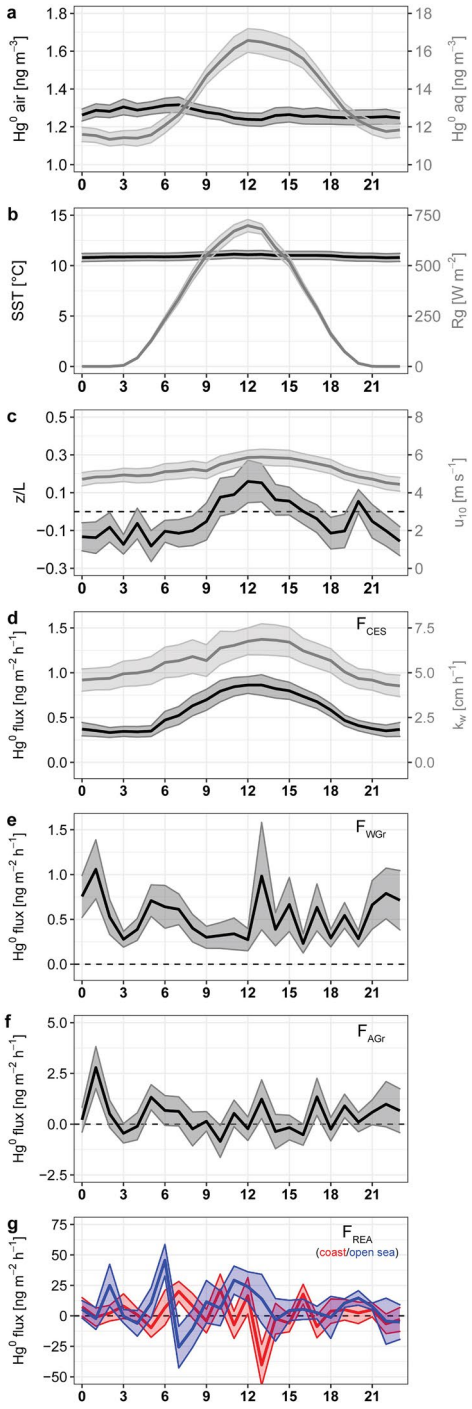

Figure 4. Diel patterns of environmental parameters and modeled and measured Hg^0 fluxes. Diel variation (hourly mean ± standard error) is given for: (a) Hg^0 concentrations in air (7 m level) and water, (b) sea surface temperature and solar radiation, (c) surface layer stability parameter and wind speed at 10 m height, (d) Hg^0 flux derived from the continuous equilibrium system and the water-side gas transfer velocity (k_w) used in the gas exchange model, (e) Hg^0 flux derived from the water-side gradient-based method, (f) Hg^0 flux calculated based on the aerodynamic gradient method, and (g) Hg^0 flux measured with the relaxed eddy accumulation system (coastal and open sea flux in red and blue, respectively). Open sea conditions: 80° < WD < 160°. Coastal conditions: 160° < WD < 220°.

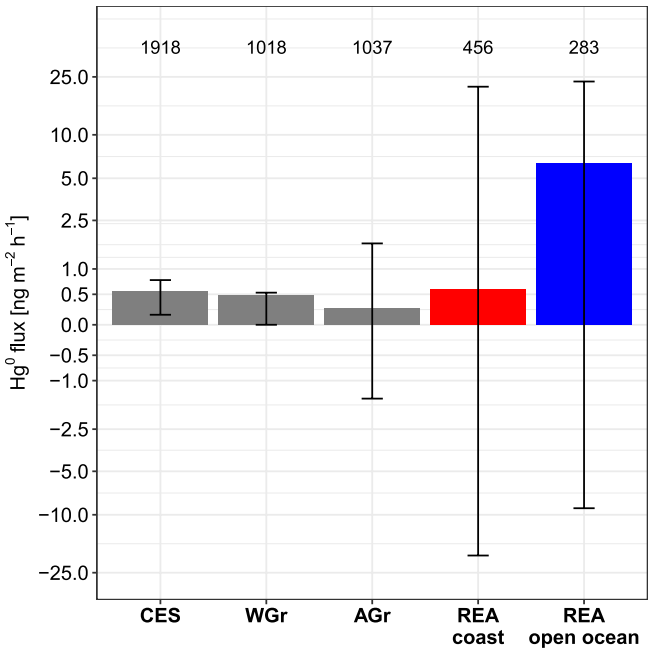

Figure 5. Overview of mean Hg^0 fluxes. The fluxes are calculated using the continuous equilibrium system, the water-side gradient approach, the aerodynamic gradient method, and the relaxed eddy accumulation (REA) technique. The Hg^0 fluxes derived from the REA system are indicated for coastal (160° < WD < 220°) and open sea (80° < WD < 160°) conditions. Number of observations are given. The error bars indicate the 25th and 75th percentiles.

7.7 m s^{-1} for coastal conditions. The predominance of such lower wind speeds in the entire data set made it difficult to discern distinctions in the relationship between k_{Hg} and higher wind speeds when open sea or coastal conditions prevailed. The subset of Hg^0 emission data covered a two day period (June 06–07, 2017) with stationary conditions representing the open sea, a Hg^0_{aq} saturation varying between 150% and 410%, and a wide range in wind speed (3.0–14.7 m s^{-1}). Even though our data set was limited ($n = 12$), we found a cubic relation ($k_{Hg} = 0.18 u_{10}^3$) between k_{Hg} ($k_{Hg} < 300$ cm h^{-1}) and wind speed for the open sea sector ($r^2 = 0.95$, $p < 0.05$; Figure 6).

3.8. Meteorological Hg^0 Flux Variability

The range in the Hg^0 flux among the three meteorological methods (F_{WGr}, F_{AGr}, F_{REA}), measured during periods when wind directions from the coastal sector prevailed, increased from 0–2.1 ng m^{-2} h^{-1} for F_{WGr}, to −3.8–5.6 ng m^{-2} h^{-1} for F_{AGr} and to −45–40 ng m^{-2} h^{-1} for F_{REA}. The sampling variability in Hg^0 fluxes for coastal conditions was further assessed by hourly averaged cumulative fluxes for each day. The Hg^0 fluxes were 0.5 ± 0.2 μg m^{-2} $month^{-1}$ (F_{WGr}), 0.4 ± 0.8 μg m^{-2} $month^{-1}$ (F_{AGr}) and 0.4 ± 6.0 μg m^{-2} $month^{-1}$ (F_{REA}). The large upward and downward Hg^0 fluxes for F_{REA} can to some extent be described by the randomness of atmospheric turbulence forming the basis of micrometeorological measurements. The increasing flux variability ($F_{WGr} < F_{AGr} < F_{REA}$) indicated substantial instrumental and methodological differences between the three approaches that was underlined by a statistical analysis showing only weak correlations between F_{WGr} and F_{REA} as well F_{AGr} and F_{REA} (see Table S2 and Figure S3 in the Supporting Information). We emphasize that micrometeorological measurements of Hg^0 flux across both the air-sea interface and the air-soil interface remain challenging especially due to the low Hg^0_{air} concentration gradients that have to be resolved.

4. Discussion

4.1. Dynamics of Hg^0 Flux From Coastal Waters

The mean Hg^0 flux calculated based on results from the gas exchange model ($F_{CES} = 0.6 \pm 0.6$ ng m^{-2} h^{-1}), gradient-based methods ($F_{WGr} = 0.5 \pm 1.1$ ng m^{-2} h^{-1} and $F_{AGr} = 0.3 \pm 3.9$ ng m^{-2} h^{-1}) and relaxed eddy accumulation technique ($F_{REA} = 0.6 \pm 37$ ng m^{-2} h^{-1}) were similar for the period from May 10 to June 20, 2017 (Figure 5). These Hg^0 flux measurements, which we consider representative for the coastal Baltic Sea, were also similar to the average spring Hg^0 flux of 0.5 ng m^{-2} h^{-1} predicted for the Baltic Sea by coupled regional chemistry transport modeling (Bieser & Schrum, 2016). However, our mean Hg^0 flux measurements, ranging from 0.3 to 0.6 ng m^{-2} h^{-1}, were lower than the average Baltic Sea fluxes reported in spring (0.9 ng m^{-2} h^{-1}) and summer (1.6 ng m^{-2} h^{-1}) over a period from 2006 to 2015 (Kuss et al., 2018). The mean Hg^0 fluxes obtained in this study were also lower compared to recently measured fluxes (May to August, 2010–2019) from other border and marginal seas and coastal waters at non-contaminated sites with background Hg^0_{air} levels, such as Yellow Sea (mean = 1.1 ng m^{-2} h^{-1}), East China Sea (mean = 4.6 ng m^{-2} h^{-1}), South China Sea (mean = 5 ng m^{-2} h^{-1}), Western and Northwestern Mediterranean Sea (mean = 5.3 and 5.0, respectively) (Ci et al., 2015; Cossa et al., 2018; Nerentorp Mastromonaco, Gårdfeldt, & Wängberg 2017; Wang et al., 2016, 2019). When we consider the measurements at a diel resolution, we find that fluxes measured with micrometeorological techniques differ from those calculated with the gas exchange model by the absence of both midday Hg^0 flux peaks and regularly occurring events of seawater Hg^0 uptake (Figures 4d–4g).

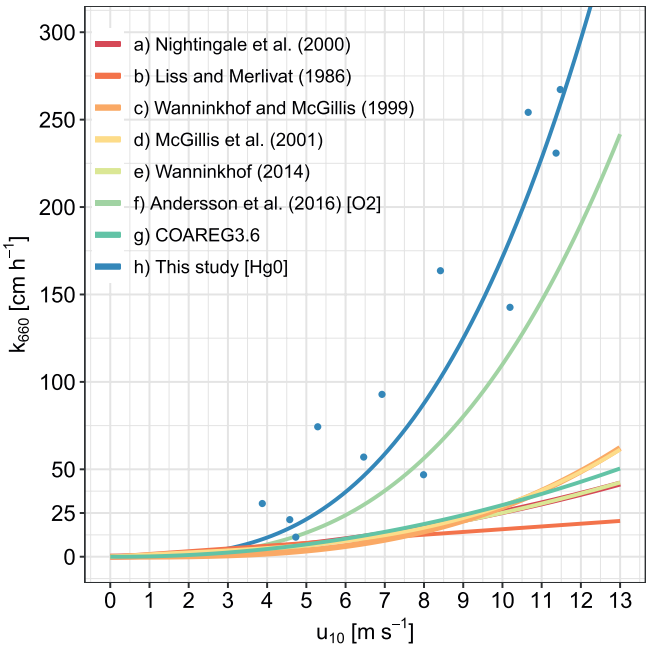

Figure 6. Wind speed dependence of transfer velocities (k_{666}) used in gas exchange models to calculate air-sea fluxes. The *k*-values are normalized to Schmidt number of 660 (20°C for CO_2 in seawater) and displayed against horizontal wind speed at 10 m [u_{10}]. The blue solid line displays the cubic fit ($k = 0.18\ u_{10}^3$) to the measured transfer velocities of Hg^0 during two days of relaxed eddy accumulation Hg^0 emission measurements (blue dots). For comparison, other wind speed relationships of the transfer velocity calculated by Nightingale et al. (2000), Liss and Merlivat (1986), Wanninkhof and McGillis (1999), McGillis et al. (2001), Wanninkhof (2014), Andersson et al. (2016) and by the Coupled Ocean-Atmosphere Response Experiment flux algorithm with CO2 model (Fairall et al., 2011) are included.

4.1.1. Interpretation of Diel Hg^0 Flux Patterns

The Hg^0 flux calculated by the gas exchange model indicated a strong diel variation (Figure 4d) while no peak is detected when using micrometeorological methods (Figures 4e–4g). Our statistical analysis found that temporal dynamics in the coastal Hg^0_{aq} concentration were a main driver of the Hg^0 flux when applying the gas exchange model (Figure 4a). The main control on coastal Hg^0_{aq} concentration was solar radiation ($\rho = 0.54$, $p < 0.05$), while SST showed a weak positive ($\rho = 0.21$, $p < 0.05$) and wind speed a weak negative correlation ($\rho = -0.15$, $p < 0.05$) with the Hg^0_{aq} concentration (see Table S2 in the Supporting Information). The statistical findings are in line with previous studies that explain the positive correlation between Hg^0_{aq} and solar radiation as a function of a photochemically driven net reduction of Hg^{II} to Hg^0 (Andersson et al., 2007; Dill et al., 2006; Gårdfeldt et al., 2003). According to the theory of the gas exchange model, this will lead to a net positive Hg^0 flux during daytime (Amyot et al., 1997; Amyot et al., 2000; Rolfhus & Fitzgerald, 2004). It has previously been shown though that elevated Hg^0_{aq}, and therefore the Hg^0 flux predicted by the model, only develop during daytime over shallow waters close to the coast with elevated SST during the day (Nerentorp Mastromonaco, Gårdfeldt, & Wängberg 2017). This is likely because of the influence of sunlight penetrating the whole water column at shallow waters and efficiently promoting net Hg^0_{aq} production when there is less wind driven mixing of the marine boundary layer.

While the gas exchange model predicts diel variability in the flux at our coastal research site our micrometeorological methods suggest that in reality this is not the case. The Hg^0 flux peaks predicted around noon by the model were not detected by the micrometeorological methods. We believe this is because the actual fluxes are influenced by variables not used to parameterize the gas exchange model (Figure 2). The actual Hg^0 fluxes are influenced not only by the Hg^0_{aq} concentrations and wind speeds in the gas exchange model but also by other factors like biological film conditions or atmospheric stability.

A change from unstable to stable marine surface layer conditions can suppress Hg^0 emission during daytime (Figure 4c). Typically, air temperatures exceeded sea surface temperatures around noon inducing stable atmospheric surface layer conditions (Figure 4b). The surface layer conditions were assessed via the unitless stability index z/L. The parameter *z* indicates the height of the sonic anemometer (10 m), and *L* represents the Obukhov length. Atmospheric stability is considered neutral when z/L ~ 0 (Zemmelink et al., 2004). Stable conditions (z/L > 0) occurred between 10:30 to 16:00 and unstable conditions (z/L < 0) between 16:00 and 10:30 (Figure 4c). Our results from the use of the micrometeorological methods thus put into question the use of the gas exchange model for coastal areas but more measurements are needed to validate these observations.

4.1.2. Seawater Hg^0 Uptake

In contrast to the gas exchange model, the aerodynamic gradient and REA measurements indicate periods of net Hg^0 uptake to coastal surface waters (53% and 45% of the time, respectively). Periods of net Hg^0 uptake have been observed in multiple studies (Mason et al., 1998; Mason et al., 2017; Soerensen et al., 2010) and explained by minima of Hg^0_{aq}, SST and Hg_{tot}, maxima of Hg^0_{air}, nitrate and nitrite concentrations as well as stimulated primary production indicated by higher chlorophyll (a) concentrations (Tseng et al., 2013). Our micrometeorological measurements likely reflect short-term variability of Hg^0_{aq} within the flux footprint that allows Hg^0 diffusion from the atmosphere into the coastal waters of the Baltic Sea. We suspect algae blooms, that were observed along the coast in Östergarnsholm during the entire measurement campaign, to play a significant role in Hg^0 uptake. Marine bloom-forming phytoplankton take up CO_2 dissolved in water during photosynthesis and account for approximately 50% of the global primary production (Falkowski

et al., 1998). Along with CO_2, a passive uptake of Hg^0 might be an important pathway for Hg accumulation in phytoplankton, a process that has been evidenced for chloride complexes ($HgCl_2$ and CH_3HgCl) (Bravo et al., 2014; Mason et al., 1996). Furthermore, biological surface films (surfactants, slicks) occurring at the sea surface microlayer have been reported to act as a barrier to air-sea gas exchange mainly because they alter the turbulent gas transfer (Frew et al., 2004; Garbe et al., 2014). We assume that surfactants slow down both the upward and downward flux of Hg^0. If biological surface films cause Hg^0 to diverge from a normal diffusion pattern, we cannot expect that Hg^0 fluxes derived from the gas exchange model and the micrometeorological methods to be similar.

4.2. Difference Between Coastal and Open Sea Hg^0 Flux

Based on the REA method, the mean open sea Hg^0 flux (6.3 ± 36 ng m^{-2} h^{-1}) was elevated ($p < 0.05$) compared to the coastal Hg^0 flux (0.6 ± 37 ng m^{-2} h^{-1}) (Figure 5). Even though positive relationships between Hg^0 fluxes and solar radiation have previously been observed in coastal areas (Andersson et al., 2007; Dill et al., 2006; Gårdfeldt et al., 2003), our Hg^0 flux measurements revealed that less than 5% ($r^2 < 0.05$, $p > 0.05$) of the variability in the measured coastal and open sea Hg^0 fluxes could be explained by solar radiation. This was also the case for other parameters used in the gas exchange model such as SST, wind speed, atmospheric pressure, salinity and Hg^0_{aq} concentrations. None of the small differences in the tested parameters can explain the order of a magnitude difference between the costal and open sea Hg^0 flux. Previous results support this conclusion indicating that there was no difference in parameters such as atmospheric turbulence or heat flux between the two sectors "coast" and "open sea" (Rutgersson et al., 2020). However, we assume that sea spray aerosol fluxes increased Hg^0 emission from the open sea sector and that biological surface films along the coast decreased Hg^0 emission from the coastal sector.

Rutgersson et al. (2020) reported a strong positive median sea spray aerosol flux from the open sea sector ($7.35 \cdot 10^5$ m^{-2} s^{-1}) and a negative aerosol flux from the costal sector ($-3.49 \cdot 10^5$ m^{-2} s^{-1}) using a condensation particle counter at wind speeds above 4 m s^{-1}. The exponential increase in upward aerosol fluxes as a function of wind speed was in agreement with results from the Arctic (Nilsson et al., 2001) and the Atlantic Ocean (Geever et al., 2005). We have reason to suspect that similar processes that enhance sea spray aerosol emissions can also increase Hg^0 emission, which could help explain the larger open sea Hg^0 emission.

On the other hand, the lower net Hg^0 flux observed at the coast could be explained by a reduced gas transfer velocity if biological surface film is present (Broecker et al., 1978). Frew (1997) found that increased surfactant abundance and dissolved organic carbon (DOC) content decreased the gas transfer velocity close to the New England coast by up to 70% compared to the open sea. Another study showed that air-sea exchange of CO_2 in the Atlantic Ocean decreased by 32% when surfactants were present (Pereira et al., 2018). Inclusion of biological surface film abundance (DOC content as a proxy) in air-sea exchange calculations from the shelf area in the West Atlantic decreased Hg^0 emission by 35%–40% (Soerensen et al., 2013). We conclude that large surfactant abundance, previously reported along the coast of Östergarnsholm (Rutgersson et al., 2011), significantly reduced coastal Hg^0 emission in our study. In order to satisfactorily explain the measured difference between coastal and open sea Hg^0 emission we need to improve our understanding of how surfactants and wind speed interact (e.g., sea spray aerosol emissions, surfactant abundance) to affect k_{Hg} and subsequently the net Hg^0 flux.

4.3. Cubic Wind Speed Dependence of k_{Hg} for the Open Sea

Our calculation of the Hg^0 transfer velocity ($k_{Hg} = 0.18 u_{10^3}$) was inconsistent with the k parameterization in Nightingale et al. (2000) ($k_w = 0.222 \cdot u_{10}^2 + 0.333 \cdot u_{10}$) that is applied in the gas exchange model for Hg^0 (Figure 6). Other frequently used wind speed relationships of the gas transfer velocity have been proposed by Liss and Merlivat (1986) ($k_w = 2.8 \cdot u_{10} - 9.6$, for $3.6 < u_{10} < 13$ m s^{-1}), Wanninkhof and McGillis (1999) ($k_w = 0.0283 \cdot u_{10}^3$), McGillis et al. (2001) ($k_w = 3.3 + 0.026 \cdot u_{10}^3$) and Wanninkhof (2014) ($k_w = 0.251 \cdot u_{10}^2$). The fit through the data from COAREG3.6 algorithm output was $k_w = 0.04 \cdot u_{10}^3 - 0.333 \cdot u_{10}^2 + 2.168 u_{10}$. While the k_{Hg} derived in this study differs significantly from the above presented coefficients it resembles the cubic gas transfer parameterization for O_2 (Figure 6). Andersson et al. (2016) calculated the O_2 transfer

velocity ($k_{O_2} = 0.11 \cdot u_{10}^3$) based on eddy covariance flux measurements over a period of six days (September 26, 2011 and June 20–24, 2013) at the same research site used in this study. Both Hg^0 (45 μg L^{-1} at 20°C) and O_2 (9.1 mg L^{-1} at 20°C) have a lower solubility than CO_2 (1.7 g L^{-1} at 20°C). The different gas transfer velocity equations in the literature based on in-situ measurements indicate that additional forcing factors such as wave breaking and bubble formation lead to different transfer properties for different gases (Garbe et al., 2014).

Our data suggest that for wind speeds higher than circa 5 m s^{-1} the k_{Hg} shows a stronger wind dependency compared to more soluble gases such as CO_2. The stronger wind dependence of k_{Hg} and k_{O2} coincides with the finding that transfer velocities of less soluble gases are enhanced by small scale waves and that bubble formation becomes more effective at higher wind speeds (>5 m s^{-1}) (Liss & Merlivat, 1986). Bubble formation enhances the gas transfer velocity (Keeling, 1993; D. K. Woolf, 1993) and was inversely proportional to the gas solubility (Asher, 1997; Asher & Wanninkhof, 1998; D. Woolf, 1997). Subsequently, the onset of small scale wave breaking (>5 m s^{-1} at our site; visual inspection) and bubble mediated transfer is suggested to accelerate the transfer velocity of Hg^0 and O_2 compared to CO_2 or DMS (Kitaigorodskii & Donelan, 1984; D. K. Woolf, 2005). However, the parameterization of bubbles created in the wave breaking process is challenging and shows large regional differences especially between the open sea and coastal waters (Callaghan et al., 2008; D. K. Woolf, 2005).

The cubic wind dependence of k_{Hg} compared to the commonly used quadratic k-parameterization implies that we might underestimate Hg^0 emission when winds are high enough for waves to start breaking. Detailed simultaneous measurements of k_{Hg} and k_{CO2} are also required to better understand the importance of bubble-mediated air-sea Hg^0 exchange (Bell et al., 2017). When we apply $k_{Hg} = 0.18 \cdot u_{10}^3$ instead of $k_w = 0.222 \cdot u_{10}^2 + 0.333 \cdot u_{10}$, the mean Hg^0 flux for the coastal Baltic Sea was 2.6 ± 4.4 ng m^{-2} h^{-1} (more than four times greater than for the quadratic parameterization). To exemplify the consequences of using different parameterizations of k (Zhang et al., 2019), the mean coastal Baltic Sea Hg^0 flux was 0.3 ± 0.6 ng m^{-2} h^{-1} for wind speeds 10 m above the ocean surface in the interval 3.6 < u10 < 13 m s^{-1} when using Liss and Merlivat, (1986), 0.4 ± 0.7 ng m^{-2} h^{-1} for Wanninkhof and McGillis (1999), 0.6 ± 0.7 ng m^{-2} h^{-1} for McGillis et al., (2001), 0.5 ± 0.6 ng m^{-2} h^{-1} for Wanninkhof (2014) and 0.6 ± 0.7 ng m^{-2} h^{-1} when applying COAREG3.6 Already at wind speeds beyond circa 5 m s^{-1}, the application of the cubic REA k-parameterization would strongly increase the Hg^0 flux in high-wind-speed regions, especially in the high latitudes. We suggest not to extrapolate the Hg^0 flux for wind speeds over 12 m s^{-1} since that was the maximum of the observational range used to parameterize k_{Hg} in this study. However, before we are able to discuss consequences of using a cubic wind speed parameterizations of k_{Hg} in detail, we need more long-term, direct Hg^0 flux measurements, across a greater range of wind speeds. The recent presentation of the first eddy covariance system with sufficient accuracy to measure Hg^0 land-atmosphere exchange over natural surfaces (Osterwalder et al., 2020) might be more easily applied to measure air-sea Hg^0 exchange than the more technically challenging REA method used in this study. Before applying this novel eddy covariance method for Hg over oceans, though, the accuracy will need to be improved compared to what was achieved in the premier application of this method, given the generally lower gradients over water than land.

5. Conclusions

With this study we address the call of the Minamata Convention (UNEP, 2013) to improve our understanding of air-sea exchange of Hg^0 by providing a comparison between modeled and measured Hg^0 fluxes. The mean coastal Hg^0 flux of 0.6 ng m^{-2} h^{-1} derived from the gas exchange model (May 10 to June 20, 2018) was equal to the annual average flux rate estimated using a coupled physical-biogeochemical model for the Baltic Sea (Soerensen et al., 2016) but was lower compared to other in situ flux measurements in coastal margin seas (Sommar et al., 2020). Concurrent micrometeorological Hg^0 flux measurements representative for the coastal Baltic Sea revealed a mean flux very similar to the modeled flux. Fluxes measured with aerodynamic gradient and REA methods, however, showed that seawater Hg^0 uptake occurred frequently (~50% of the time) also during periods when the gas exchange model indicated Hg^0 evasion (which was 99% of the time). A subset of Hg^0 evasion data representative for open sea conditions measured with the REA method indicated a stronger wind dependence of k_{Hg} than other commonly used parameterizations for Hg^0. Our

data indicate that air-sea exchange of Hg^0 becomes more efficient at wind speeds of about 5 m s^{-1}, which may be related to the low solubility of Hg^0. Thus, we highlight the need to follow up on the transfer velocity (k_{Hg}) – wind speed relationship determined from direct Hg^0 flux measurements to improve quantitative knowledge of the air-sea exchange, especially during periods when wind speeds are high enough for waves to start breaking. At the same time we propose an implementation of the Hg^0 transfer velocity code into the COAREG physically based bulk flux algorithm that could be capable of capturing the effect of Hg^0 solubility that may be responsible for the cubic wind speed dependence. We need multi-seasonal Hg^0 flux time series to make statistically significant estimates of the dependence of fluxes on other environmental parameters, including complementary observations relevant to hypothesized explanations such as the role of sea spray aerosol emission, occurrence of biological surface films or bubble formation. This can be done with direct Hg^0 flux measurements on islands, floating instrument platforms or research vessels using the newly available eddy covariance technique (Osterwalder et al., 2020). If there is indeed a stronger cubic wind speed dependence for k_{Hg}, similar to that of O_2 which also has low solubility, there will be a need to reevaluate the understanding and modeling of Hg^0 flux processes at local, regional and global scales.

Conflict of Interest

The authors declare that they have no conflict of interest.

Data Availability Statement

The basic data used in this paper are made available through a community data repository (https://www.safedeposit.se/projects/305).

Acknowledgments
The research was funded by the Swedish Research Council through the Sino-Swedish Mercury Management Research Framework (SMaReF Dnr 639-2013-6978) and the Swedish research infrastructures ICOS and SITES. The ICOS station Östergarnsholm is funded by the Swedish Research Council (grants 2012-03902 and 2013-02044) and Uppsala University. S. Osterwalder received funding for data analysis and manuscript writing from the Research Fund for Junior Researchers of the University of Basel and the Swiss National Science Foundation grant P400P2_180796. W. Zhu acknowledges additional financial support from the Swedish Research Council Formas (2017-01085). M. Jiskra received funding from the H2020 Marie Sklodowska-Curie grant No 657195 and Swiss National Science Foundation grant PZ00P2_174101. Special thanks go to Dr. Johannes Fritsche for supporting analysis of gradient-based and REA flux measurements. We want to acknowledge all technical staff and researchers involved in the study supporting the measurement campaign at ICOS Östergarnsholm.

References

Amos, H. M., Jacob, D. J., Streets, D. G., & Sunderland, E. M. (2013). Legacy impacts of all-time anthropogenic emissions on the global mercury cycle. *Global Biogeochemical Cycles*, *27*, 410–421. https://doi.org/10.1002/gbc.20040

Amyot, M., Gill, G. A., & Morel, F. M. M. (1997). Production and loss of dissolved gaseous mercury in coastal seawater. *Environmental Science & Technology*, *31*, 3606–3611. https://doi.org/10.1021/es9703685

Amyot, M., Lean, D. R. S., Poissant, L., & Doyon, M.-R. (2000). Distribution and transformation of elemental mercury in the St. Lawrence River and Lake Ontario. *Canadian Journal of Fisheries and Aquatic Sciences*, *57*(S1), 155–163. https://doi.org/10.1139/f99-248

Andersson, A., Rutgersson, A., & Sahlée, E. (2016). Using eddy covariance to estimate air–sea gas transfer velocity for oxygen. *Journal of Marine Systems*, *159*, 67–75. https://doi.org/10.1016/j.jmarsys.2016.02.008

Andersson, M. E., Gårdfeldt, K., & Wängberg, I. (2008). A description of an automatic continuous equilibrium system for the measurement of dissolved gaseous mercury. *Analytical and Bioanalytical Chemistry*, *391*, 2277–2282. https://doi.org/10.1007/s00216-008-2127-4

Andersson, M. E., Gårdfeldt, K., Wängberg, I., Sprovieri, F., Pirrone, N., & Lindqvist, O. (2007). Seasonal and daily variation of mercury evasion at coastal and off shore sites from the Mediterranean Sea. *Marine Chemistry*, *104*, 214–226. https://doi.org/10.1016/j.marchem.2006.11.003

Andersson, M. E., Gårdfeldt, K., Wängberg, I., & Strömberg, D. (2008). Determination of Henry's Law constant for elemental mercury. *Chemosphere*, *73*(4), 587–592. https://doi.org/10.1016/j.chemosphere.2008.05.067

Asher, W. E. (1997). The sea-surface microlayer and its effect on global air-sea gas transfer. In P. S. Liss, & R. A. Duce (Eds.), *The sea surface and global change* (pp. 251–286). Cambridge University Press. https://doi.org/10.1017/cbo9780511525025.009

Asher, W. E., & Wanninkhof, R. (1998). The effect of bubble-mediated gas transfer on purposeful dual-gaseous tracer experiments. *Journal of Geophysical Research*, *103*, 10555–10560. https://doi.org/10.1029/98JC00245

Bell, T. G., Landwehr, S., Miller, S. D., de Bruyn, W. J., Callaghan, A. H., Scanlon, B., et al. (2017). Estimation of bubble-mediated air–sea gas exchange from concurrent DMS and CO_2 transfer velocities at intermediate–high wind speeds. *Atmospheric Chemistry and Physics*, *17*, 9019–9033. https://doi.org/10.5194/acp-17-9019-2017

Bieser, J., & Schrum, C. (2016). Impact of marine mercury cycling on coastal atmospheric mercury concentrations in the North- and Baltic Sea region. *ELEMENTA Science of the Anthropocene*, *4*, 000111. https://doi.org/10.12952/journal.elementa.000111

Bravo, A. G., Le Faucheur, S., Monperrus, M., Amouroux, D., & Slaveykova, V. I. (2014). Species-specific isotope tracers to study the accumulation and biotransformation of mixtures of inorganic and methyl mercury by the microalga Chlamydomonas reinhardtii. *Environmetnal Pollution*, *192*, 212–215. https://doi.org/10.1016/j.envpol.2014.05.013

Broecker, H.-C., Petermann, J., & Siems, W. (1978). The influence of wind on CO_2 exchange in a wind wave tunnel, including the effects of monolayers. *Journal of Marine Research*, *36*(4), 595–610.

Callaghan, A., de Leeuw, G., Cohen, L., & O'Dowd, C. D. (2008). Relationship of oceanic whitecap coverage to wind speed and wind history. *Geophysical Research Letters*, *35*, L23609. https://doi.org/10.1029/2008GL036165

Ci, Z. J., Wang, C. J., Wang, Z. W., & Zhang, X. S. (2015). Elemental mercury (Hg(0)) in air and surface waters of the Yellow Sea during late spring and late fall 2012: Concentration, spatial-temporal distribution and air/sea flux. *Chemosphere*, *119*, 199–208. https://doi.org/10.1016/j.chemosphere.2014.05.064

Converse, A. D., Riscassi, A. L., & Scanlon, T. M. (2010). Seasonal variability in gaseous mercury fluxes measured in a high-elevation meadow. *Atmospheric Environment*, *44*, 2176–2185. https://doi.org/10.1016/j.atmosenv.2010.03.024

Cossa, D., Durrieu de Madron, X., Schäfer, J., Guédron, S., Marusczak, N., Castelle, S., & Naudin, J.-J. (2018). Sources and exchanges of mercury in the waters of the Northwestern Mediterranean margin, Special issue of MERMEX project: Recent advances in the oceanography of the Mediterranean Sea. *Progress in Oceanography*, *163*, 172–183. https://doi.org/10.1016/j.pocean.2017.05.002

Dill, C., Kuiken, T., Zhang, H., & Ensor, M. (2006). Diurnal variation of dissolved gaseous mercury (DGM) levels in a southern reservoir lake (Tennessee, USA) in relation to solar radiation. *Science of the Total Environment*, *357*, 176–193. https://doi.org/10.1016/j.scitotenv.2005.04.011

Edwards, G. C., Rasmussen, P. E., Schroeder, W. H., Wallace, D. M., Halfpenny-Mitchell, L., Dias, G. M., et al. (2005). Development and evaluation of a sampling system to determine gaseous Mercury fluxes using an aerodynamic micrometeorological gradient method. *Journal of Geophysical Research*, *110*. https://doi.org/10.1029/2004JD005187

Fairall, C. W., Yang, M., Bariteau, L., Edson, J. B., Helmig, D., McGillis, W., et al. (2011). Implementation of the Coupled Ocean-Atmosphere Response Experiment flux algorithm with CO_2, dimethyl sulfide, and O_3. *Journal of Geophysical Research*, *116*, C00F09. https://doi.org/10.1029/2010JC006884

Falkowski, P. G., Barber, R. T., & Smetacek, V. (1998). Biogeochemical controls and feedbacks on ocean primary production. *Science*, *281*, 200–206. https://doi.org/10.1126/science.281.5374.200

Fantozzi, L., Manca, G., & Sprovieri, F. (2013). A comparison of recent methods for modeling mercury fluxes at the air-water interface. *E3S Web of Conferences*, *1*, 23004. https://doi.org/10.1051/e3sconf/20130123004

Foken, T., & Wichura, B. (1996). Tools for quality assessment of surface based flux measurements. *Agricultural and Forest Meteorology*, *78*, 83–105. https://doi.org/10.1016/0168-1923(95)02248-1

Frew, N. M. (1997). The role of organic films in air-sea gas exchange. In P. S. Liss, & R. A. Duce (Eds.), *The Sea surface and global change* (pp. 121–172). Cambridge University Press. https://doi.org/10.1017/cbo9780511525025.006

Frew, N. M., Bock, E. J., Schimpf, U., Hara, T., Haußecker, H., Edson, J. B., et al. (2004). Air-sea gas transfer: Its dependence on wind stress, small-scale roughness, and surface films. *Journal of Geophysical Research*, *109*, C08S17. https://doi.org/10.1029/2003JC002131

Fritsche, J., Obrist, D., Zeeman, M. J., Conen, F., Eugster, W., & Alewell, C. (2008). Elemental mercury fluxes over a sub-alpine grassland determined with two micrometeorological methods. *Atmospheric Environment*, *42*, 2922–2933. https://doi.org/10.1016/j.atmosenv.2007.12.055

Garbe, C. S., Rutgersson, A., Boutin, J., de Leeuw, G., Delille, B., Fairall, C. W., et al. (2014). Transfer across the air-sea interface. In P. S. Liss, & M. T. Johnson (Eds.), *Ocean-Atmosphere interactions of gases and particles* (pp. 55–112). Springer Earth System Sciences: Springer. https://doi.org/10.1007/978-3-642-25643-1_2

Gårdfeldt, K., Horvat, M., Sommar, J., Kotnik, J., Fajon, V., Wängberg, I., & Lindqvist, O. (2002). Comparison of procedures for measurements of dissolved gaseous mercury in seawater performed on a Mediterranean cruise. *Analytical and Bioanalytical Chemistry*, *374*, 1002–1008. https://doi.org/10.1007/s00216-002-1592-4

Gårdfeldt, K., Sommar, J., Ferrara, R., Ceccarini, C., Lanzillotta, E., Munthe, J., et al. (2003). Evasion of mercury from coastal and open waters of the Atlantic Ocean and the Mediterranean Sea. *Atmospheric Environment*, *37*, 73–84. https://doi.org/10.1016/S1352-2310(03)00238-3

Geever, M., O'Dowd, C. D., van Ekeren, S., Flanagan, R., Nilsson, E. D., de Leeuw, G., & Rannik, Ü. (2005). Submicron sea spray fluxes. *Geophysical Research Letters*, *32*. https://doi.org/10.1029/2005GL023081

Grönholm, T., Haapanala, S., Launiainen, S., Rinne, J., Vesala, T., & Rannik, U. (2008). The dependence of the beta coefficient of REA system with dynamic deadband on atmospheric conditions. *Environmental Pollution*, *152*, 597–603. https://doi.org/10.1016/j.envpol.2007.06.071

Gualtieri, D., & Mihailović, C. (2008). *Fluid mechanics of environmental interfaces*. Taylor & Francis Group (ISBN: 0-203-89535-5 Master e-book ISBN).

Hintsa, E. J., Dacey, J. W. H., McGillis, W. R., Edson, J. B., Zappa, C. J., & Zemmelink, H. J. (2004). Sea-to-air fluxes from measurements of the atmospheric gradient of dimethylsulfide and comparison with simultaneous relaxed eddy accumulation measurements. *Journal of Geophysical Research*, *109*, C01026. https://doi.org/10.1029/2002JC001617

Hoglind, H., Eriksson, S., & Gårdfeldt, K. (2018). Ship-based measurements of atmospheric mercury concentrations over the Baltic Sea. *Atmosphere*, *9*, 56. https://doi.org/10.3390/atmos9020056

Holmes, C. D., Jacob, D. J., Mason, R. P., & Jaffe, D. A. (2009). Sources and deposition of reactive gaseous mercury in the marine atmosphere. *Atmospheric Environment*, *43*(14), 2278–2285. https://doi.org/10.1016/j.atmosenv.2009.01.051

Honkanen, M., Tuovinen, J.-P., Laurila, T., Mäkelä, T., Hatakka, J., Kielosto, S., & Laakso, L. (2018). Measuring turbulent CO_2 fluxes with a closed-path gas analyzer in a marine environment. *Atmospheric Measurement Techniques*, *11*, 5335–5350. https://doi.org/10.5194/amt-11-5335-2018

Horowitz, H. M., Jacob, D. J., Zhang, Y., Dibble, T. S., Slemr, F., Amos, H. M., et al. (2017). A new mechanism for atmospheric mercury redox chemistry: Implications for the global mercury budget. *Atmospheric Chemistry and Physics*, *17*, 6353–6371. https://doi.org/10.5194/acp-17-6353-2017

Johnson, M. T. (2010). A numerical scheme to calculate temperature and salinity dependent air-water transfer velocities for any gas. *Ocean Science*, *6*, 913–932. https://doi.org/10.5194/os-6-913-2010

Keeling, R. F. (1993). On the role of large bubbles in air-sea gas exchange and supersaturation in the ocean. *Journal of Marine Research*, *51*, 237–271. https://doi.org/10.1357/0022240933223800

Kitaigorodskii, S., & Donelan, M. A. (1984). Wind-wave effects on gas transfer. In W. Brutsaert, G. H. Jirka, & D. Reidel (Eds.), *Gas transfer at water surfaces* (pp. 147–170). https://doi.org/10.1007/978-94-017-1660-4_14

Kuss, J. (2014). Water-air gas exchange of elemental mercury: An experimentally determined mercury diffusion coefficient for Hg0 water-air flux calculations. *Limnology & Oceanography*, *59*, 1461–1467. https://doi.org/10.4319/lo.2014.59.5.1461

Kuss, J., Krüger, S., Ruickoldt, J., & Wlost, K.-P. (2018). High-resolution measurements of elemental mercury in surface water for an improved quantitative understanding of the Baltic Sea as a source of atmospheric mercury. *Atmospheric Chemistry and Physics*, *18*, 4361–4376. https://doi.org/10.5194/acp-18-4361-2018

Lavoie, R. A., Jardine, T. D., Chumchal, M. M., Kidd, K. A., & Campbell, L. M. (2013). Biomagnification of mercury in aquatic food webs: A Worldwide meta-analysis. *Environmental Science & Technology*, *47*(23), 13385–13394. https://doi.org/10.1021/es403103t

Leppäranta, M., & Myrberg, K. (2009). *Physical oceanography of the Baltic Sea*. Springer.

Liss, P. S., & Merlivat, L. (1986). Air-sea gas exchange rates: Introduction and synthesis. In P. Buat-Ménard (Ed.), *The role of air-sea exchange in geochemical cycling* (pp. 113–127). Springer Netherlands. https://doi.org/10.1007/978-94-009-4738-2_5

MacSween, K., Edwards, G. C., & Beggs, P. J. (2020). Seasonal gaseous elemental mercury fluxes at a terrestrial background site in south-eastern Australia. *ELEMENTA Science of the Anthropocene*, *8*, 27. https://doi.org/10.1525/elementa.423

Mason, R. P., Hammerschmidt, C. R., Lamborg, C. H., Bowman, K. L., Swarr, G. J., & Shelley, R. U. (2017). The air-sea exchange of mercury in the low latitude Pacific and Atlantic Oceans. *Deep-Sea Research Part I-Oceanographic Research Papers*, *122*, 17–28. https://doi.org/10.1016/j.dsr.2017.01.015

Mason, R. P., Reinfelder, J. R., & Morel, F. M. M. (1996). Uptake, toxicity, and trophic transfer of mercury in a coastal diatom. *Environmental Science & Technology*, *30*, 1835–1845. https://doi.org/10.1021/es950373d

Mason, R. P., Rolfhus, K. R., & Fitzgerald, W. F. (1998). Mercury in the North Atlantic. *Marine Chemistry*, *61*, 37–53. https://doi.org/10.1016/S0304-4203(98)00006-1

McGillis, W. R., Edson, J. B., Hare, J. E., & Fairall, C. W. (2001). Direct covariance air-sea CO_2 fluxes. *Journal of Geophysical Research*, *106*, 16729–16745. https://doi.org/10.1029/2000JC000506

McNeil, C., & D'Asaro, E. (2007). Parameterization of air–sea gas fluxes at extreme wind speeds. *Journal of Marine Systems*, *66*, 110–121. https://doi.org/10.1016/j.jmarsys.2006.05.013

Nerentorp Mastromonaco, M. G. (2016). Mercury cycling in the global marine environment (p. 260). Department of Chemistry and Chemical Engineering. Ph. D. Thesis Chalmers University of Technology.

Nerentorp Mastromonaco, M. G., Gårdfeldt, K., & Langer, S. (2017). Mercury flux over West Antarctic Seas during winter, spring and summer, The role of oceans in the global mercury observing systems. *Marine Chemistry*, *193*, 44–54. https://doi.org/10.1016/j.marchem.2016.08.005

Nerentorp Mastromonaco, M. G., Gårdfeldt, K., & Wängberg, I. (2017). Seasonal and spatial evasion of mercury from the western Mediterranean Sea, The role of oceans in the global mercury observing systems. *Marine Chemistry*, *193*, 34–43. https://doi.org/10.1016/j.marchem.2017.02.003

Nightingale, P. D., Malin, G., Law, C. S., Watson, A. J., Liss, P. S., Liddicoat, M. I., et al. (2000). In situ evaluation of air-sea gas exchange parameterizations using novel conservative and volatile tracers. *Global Biogeochemical Cycles*, *14*, 373–387. https://doi.org/10.1029/1999GB900091

Nilsson, E. D., Rannik, Ü., Swietlicki, E., Leck, C., Aalto, P. P., Zhou, J., & Norman, M. (2001). Turbulent aerosol fluxes over the Arctic Ocean: 2. Wind-driven sources from the sea. *Journal of Geophysical Research*, *106*, 32139–32154. https://doi.org/10.1029/2000JD900747

Osterwalder, S., Bishop, K., Alewell, C., Fritsche, J., Laudon, H., Åkerblom, S., & Nilsson, M. B. (2017). Mercury evasion from a boreal peatland shortens the timeline for recovery from legacy pollution. *Scientific Reports*, *7*, 1–9. https://doi.org/10.1038/s41598-017-16141-7

Osterwalder, S., Eugster, W., Feigenwinter, I., & Jiskra, M. (2020). Eddy covariance flux measurements of gaseous elemental mercury over a grassland. *Atmospheric Measurement Techniques*, *13*, 2057–2074. https://doi.org/10.5194/amt-13-2057-2020

Osterwalder, S., Fritsche, J., Alewell, C., Schmutz, M., Nilsson, M. B., Jocher, G., et al. (2016). A dual-inlet, single detector relaxed eddy accumulation system for long-term measurement of mercury flux. *Atmospheric Measurement Techniques*, *9*, 509–524. https://doi.org/10.5194/amt-9-509-2016

Osterwalder, S., Sommar, J., Åkerblom, S., Jocher, G., Fritsche, J., Nilsson, M. B., et al. (2018). Comparative study of elemental mercury flux measurement techniques over a Fennoscandian boreal peatland. *Atmospheric Environment*, *172*, 16–25. https://doi.org/10.1016/j.atmosenv.2017.10.025

Pereira, R., Ashton, I., Sabbaghzadeh, B., Shutler, J. D., & Upstill-Goddard, R. C. (2018). Reduced air–sea CO_2 exchange in the Atlantic Ocean due to biological surfactants. *Nature Geoscience*, *11*, 492–496. https://doi.org/10.1038/s41561-018-0136-2

Qureshi, A., MacLeod, M., Sunderland, E. M., & Konrad, H. (2011). Exchange of elemental mercury between the oceans and the atmosphere. In Liu, G., Cai, Y., & O'Driscoll, N. J. (Eds.) *Environmental chemistry and toxicology of mercury* (pp. 389–421). John Wiley & Sons, Inc. https://doi.org/10.1002/9781118146644.ch12

Rolfhus, K. R., & Fitzgerald, W. F. (2004). Mechanisms and temporal variability of dissolved gaseous mercury production in coastal seawater. *Marine Chemistry*, *90*, 125–136. https://doi.org/10.1016/j.marchem.2004.03.012

Rosentau, A., Bennike, O., Uścinowicz, S., & Miotk-Szpiganowicz, G. (2017). The Baltic Sea Basin. In *Submerged landscapes of the European continental shelf* (pp. 103–133). John Wiley & Sons, Ltd. https://doi.org/10.1002/9781118927823.ch5

Rutgersson, A., Norman, M., Schneider, B., Pettersson, H., & Sahlée, E. (2008). The annual cycle of carbon dioxide and parameters influencing the air–sea carbon exchange in the Baltic Proper. *Journal of Marine Systems*, *74*, 381–394. https://doi.org/10.1016/j.jmarsys.2008.02.005

Rutgersson, A., Pettersson, H., Nilsson, E., Bergström, H., Wallin, M. B., Nilsson, E. D., et al. (2020). Using land-based stations for air–sea interaction studies. *Tellus A: Dynamic Meteorology and Oceanography*, *72*, 1–23. https://doi.org/10.1080/16000870.2019.1697601

Rutgersson, A., Smedman, A., & Sahlée, E. (2011). Oceanic convective mixing and the impact on air-sea gas transfer velocity. *Geophysical Research Letters*, *38*, L02602. https://doi.org/10.1029/2010GL045581

Sanemasa, I. (1975). The solubility of elemental mercury-vapor in water. *Bulletin of the Chemical Society of Japan*, *48*, 1795–1798. https://doi.org/10.1246/bcsj.48.1795

Selin, N. E. (2009). Global biogeochemical cycling of mercury: A review. *Annual Review of Environment and Resources*, *34*, 43–63. https://doi.org/10.1146/annurev.environ.051308.084314

Soerensen, A. L., Mason, R. P., Balcom, P. H., Jacob, D. J., Zhang, Y., Kuss, J., & Sunderland, E. M. (2014). Elemental mercury concentrations and fluxes in the tropical atmosphere and ocean. *Environmental Science & Technology*, *48*(19), 11312–11319. https://doi.org/10.1021/es503109p

Soerensen, A. L., Mason, R. P., Balcom, P. H., & Sunderland, E. M. (2013). Drivers of surface ocean mercury concentrations and air–sea exchange in the West Atlantic Ocean. *Environmental Science & Technology*, *47*(14), 7757–7765. https://doi.org/10.1021/es401354q

Soerensen, A. L., Schartup, A. T., Gustafsson, E., Gustafsson, B. G., Undeman, E., & Björn, E. (2016). Eutrophication increases phytoplankton methylmercury concentrations in a coastal sea—A Baltic sea case study. *Environmental Science & Technology*, *50*, 11787–11796. https://doi.org/10.1021/acs.est.6b02717

Soerensen, A. L., Schartup, A. T., Skrobonja, A., Bouchet, S., Amouroux, D., Liem-Nguyen, V., & Björn, E. (2018). Deciphering the role of water column redoxclines on methylmercury cycling using speciation modeling and observations from the Baltic Sea. *Global Biogeochemical Cycles*, *32*, 1498–1513. https://doi.org/10.1029/2018GB005942

Soerensen, A. L., Sunderland, E. M., Holmes, C. D., Jacob, D. J., Yantosca, R. M., Skov, H., et al. (2010). An improved global model for air-sea exchange of mercury high concentrations over the North Atlantic. *Environmental Science & Technology*, *44*, 8574–8580. https://doi.org/10.1021/es102032g

Sommar, J., Osterwalder, S., & Zhu, W. (2020). Recent advances in understanding and measurement of Hg in the environment: Surface-atmosphere exchange of gaseous elemental mercury (Hg0). *The Science of the Total Environment*, *721*, 137648. https://doi.org/10.1016/j.scitotenv.2020.137648

Tseng, C. M., Lamborg, C. H., & Hsu, S. C. (2013). A unique seasonal pattern in dissolved elemental mercury in the South China Sea, a tropical and monsoon-dominated marginal sea. *Geophysical Research Letters*, *40*, 167–172. https://doi.org/10.1029/2012GL054457

UNEP. (2013). *Minamata convention on mercury* (p. 62). Accessed date 16 June 2020. http://www.mercuryconvention.org

UNEP. (2019). *Global mercury assessment 2018. UN environment program, chemicals and health branch*. Accessed date: 16 June 2020. https://www.unenvironment.org/resources/publication/global-mercury-assessment-2018

USEPA. (2002). Method 1631, Revision E: Mercury in water by oxidation, purge and trap, and cold vapor atomic fluorescence spectrometry. Available at https://www.epa.gov/sites/production/files/2015-08/documents/method_1631e_2002.pdf

Wang, C. J., Ci, Z. J., Wang, Z. W., & Zhang, X. S. (2016). Air-sea exchange of gaseous mercury in the East China Sea. *Environmental Pollution*, *212*, 535–543. https://doi.org/10.1016/j.envpol.2016.03.016

Wang, C. J., Wang, Z. J., Hui, F., & Zhang, X. S. (2019). Speciated atmospheric mercury and sea–air exchange of gaseous mercury in the South China Sea. *Atmospheric Chemistry and Physics*, *19*, 10111–10127. https://doi.org/10.5194/acp-19-10111-2019

Wanninkhof, R. (1992). Relationship between wind speed and gas exchange over the ocean. *Journal of Geophysical Research*, *97*, 7373–7382. https://doi.org/10.1029/92JC00188

Wanninkhof, R. (2014). Relationship between wind speed and gas exchange over the ocean revisited. *Limnology and Oceanography: Methods*, *12*, 351–362. https://doi.org/10.4319/lom.2014.12.351

Wanninkhof, R., & McGillis, W. R. (1999). A cubic relationship between air–sea CO_2 exchange and wind speed. *Geophysical Research Letters*, *26*(13), 1889–1892. https://doi.org/10.1029/1999GL900363

Whalin, L., Kim, E. H., & Mason, R. (2007). Factors influencing the oxidation, reduction, methylation and demethylation of mercury species in coastal waters. *Marine Chemistry*, *107*(3), 278–294. https://doi.org/10.1016/j.marchem.2007.04.002

Woolf, D. (1997). Bubbles and their role in air-sea gas exchange. In P. S. Liss, & R. A. Duce (Eds.), *The Sea surface and global change* (pp. 173–206). Cambridge University Press. https://doi.org/10.1017/cbo9780511525025.007

Woolf, D. K. (1993). Bubbles and the air-sea transfer velocity of gases. *Atmosphere-Ocean*, *31*, 517–540. https://doi.org/10.1080/07055900.1993.9649484

Woolf, D. K. (2005). Parametrization of gas transfer velocities and sea-state-dependent wave breaking. *Tellus B: Chemical and Physical Meteorology*, *57*, 87–94. https://doi.org/10.1111/j.1600-0889.2005.00139.x

Yang, M., Blomquist, B. W., Fairall, C. W., Archer, S. D., & Huebert, B. J. (2011). Air-sea exchange of dimethylsulfide in the Southern Ocean: Measurements from SO GasEx compared to temperate and tropical regions. *Journal of Geophysical Research*, *116*, C00F05. https://doi.org/10.1029/2010JC006526

Zemmelink, H. J., Gieskes, W. W. C., Klaassen, W., Beukema, W. J., Groot, H. W., de Baar, H. J. W., et al. (2004). Relaxed eddy accumulation measurements of the sea-to-air transfer of dimethylsulfide over the northeastern Pacific. *Journal of Geophysical Research*, *109*, C01025. https://doi.org/10.1029/2002JC001616

Zhang, Y., Horowitz, H., Wang, J., Xie, Z., Kuss, J., & Soerensen, A. L. (2019). A coupled global atmosphere-ocean model for air-sea exchange of mercury: Insights into et deposition and atmospheric redox chemistry. *Environmental Science & Technology*, *53*, 5052–5061. https://doi.org/10.1021/acs.est.8b06205

Zhang, Y., Jaeglé, L., & Thompson, L. (2014). Natural biogeochemical cycle of mercury in a global three-dimensional ocean tracer model. *Global Biogeochemical Cycles*, *28*, 553–570. https://doi.org/10.1002/2014GB004814

Zhu, W., Sommar, J., Lin, C.-J., & Feng, X. (2015). Mercury vapor air–surface exchange measured by collocated micrometeorological and enclosure methods – Part II: Bias and uncertainty analysis. *Atmospheric Chemistry and Physics*, *15*, 5359–5376. https://doi.org/10.5194/acp-15-5359-2015